U.PORTO
FEUP FACULDADE DE ENGENHARIA
UNIVERSIDADE DO PORTO

M 2023

Permeability of Hydrogen in Pipeline Steels for Green Hydrogen

João Francisco de Araújo Correia Ferreira

Dissertation Presented to the Faculty of Engineering for the Degree of Master in Materials Engineering

José Carlos Fonseca

FEUP Supervisor

Dr. Omid Emadinia

INEGI Supervisor

Porto, September 2023

This page was intentionally left blank.

_____

CANDIDATO Código

_____

TÍTULO

_____

DATA __ de _____ de _____

_____

LOCAL Faculdade de Engenharia da Universidade do Porto – Sala _____ - __:__h

_____

_____

JÚRI Presidente DEMM/FEUP

_____

Arguente DEM/FEUP

_____

Orientador DEMM/FEUP

_____

This page was intentionally left blank.

“Success is not final, failure is not fatal: It is the courage to continue that counts.”

- **Winston Churchill**

This page was intentionally left blank.

Resumo

O hidrogénio verde apresenta-se como uma alternativa limpa, relativamente aos combustíveis fósseis, e versátil, relativamente às outras tecnologias de energia verde já conhecidas.

No contexto do transporte de hidrogénio, um dos métodos mais seguros e economicamente rentáveis de mover este combustível entre pontos de produção, armazenamento e consumo, será através da utilização das redes de tubos de gás natural já instaladas na generalidade dos países europeus. Esta rede de tubos utiliza como material o aço, sendo que, no contexto português o aço utilizado é o API 5L gr. B.

Sendo o aço um material suscetível à fragilização por hidrogénio, a permeabilidade do aço ao hidrogénio poderá levar a falhas catastróficas na rede de distribuição de gás, devido ao aprisionamento de hidrogénio na malha metálica.

Neste contexto, foi utilizado o método eletroquímico, segundo a norma ASTM G 148-97, de modo a estudar a permeabilidade do aço API 5L gr. B ao hidrogénio. Neste procedimento, duas amostras planas (com diferentes espessuras) deste aço foram preparadas de modo que, um dos lados esteja preparado para a carga de hidrogénio, e o lado oposto para a deteção. No lado destinado à deteção de hidrogénio aplicou-se um fino revestimento de níquel.

As amostras foram colocadas numa célula eletroquímica, onde foi promovida a formação e carga de hidrogénio, no lado de carga, e a deteção do hidrogénio que se difunde através do aço, no lado de deteção. A carga é realizada com recurso a uma fonte de alimentação onde a corrente é controlada e a deteção efetua-se com recurso a um potenciostato com um potencial definido, onde a corrente obtida ao longo do tempo é registada.

Dos registos da corrente obtida ao longo do tempo foi possível determinar o coeficiente de difusão efetivo para as duas amostras, tendo sido obtidos os valores de 4.18 10^{-8} cm^2/s e 1.10 10^{-7} cm^2/s. Para este efeito foram utilizados 3 métodos diferentes, de modo a validar os resultados. Destes valores, foram determinadas as concentrações de hidrogénio tendo sido obtidos os valores de 2.32 10^{-5} (mol H/cm3) e 1.70 10^{-5} (mol H/cm3). Foi ainda determinado o coeficiente de difusão de malha, através do método de ajuste linear de sucessivas permeações, sendo obtido o valor de 1.11 10^{-5} cm^2/s.

O método experimental desenvolvido durante este trabalho provou-se eficaz na determinação do coeficiente de difusão efetivo do hidrogénio no aço e da determinação da sua concentração. Os valores de concentração e coeficiente de difusão efetivo obtidos foram comparados com os obtidos em trabalhos realizados noutros aços API 5L. Da comparação concluiu-se que os valores obtidos se aproximam dos reportados na bibliografia para aços API 5L.

Palavras-chave: Hidrogénio Verde; Permeação; Eletroquímica; API 5L grade B; Fragilização por Hidrogénio; Coeficiente de Difusão Efetivo; Coeficiente de Difusão de Malha.

This page was intentionally left blank.

Abstract

Green hydrogen presents itself as a clean alternative to fossil fuels and a versatile option compared to other known green energy technologies.

In the context of hydrogen transport, one of the safest and economically viable methods for moving this fuel between production, storage, and consumption points is through the use of the natural gas pipeline networks already installed in most European countries. These pipeline networks typically use steel as their material, and in the Portuguese context, the steel used is API 5L grade B.

Since steel is susceptible to hydrogen embrittlement, the permeability of steel to hydrogen can lead to catastrophic failures in the gas distribution network due to hydrogen entrapment within the metal structure.

In this context, the electrochemical method, according to ASTM G 148-97 standard, was employed to study the permeability of API 5L grade B steel to hydrogen. In this procedure, two flat samples (with different thicknesses) of this steel were prepared so that one side is prepared for hydrogen charging, and the opposite side for detection. A thin nickel coating was applied to the side intended for hydrogen detection.

The samples were placed in an electrochemical cell where the formation and charging of hydrogen occurred on the charging side and the detection of hydrogen that diffuses through the steel took place on the detection side. The charging was carried out using a power supply where the current was controlled, and detection was performed using a potentiostat with a defined potential, where the current obtained over time was recorded.

From the recorded current over time, it was possible to determine the effective diffusion coefficient for the two samples, resulting in values of 4.18 10^{-8} cm^2/s and 1.10 10^{-7} cm^2/s. For this purpose, three different methods were used to validate the results. From these values, hydrogen concentrations were determined, resulting in values of 2.32 10^{-5} (mol H/cm^3) and 1.70 10^{-5} (mol H/cm^3). The mesh diffusion coefficient was also determined using the linear fit method of successive permeations, resulting in a value of 1.11 10^{-5} cm^2/s.

The experimental method developed during this work proved to be effective in determining the effective hydrogen diffusion coefficient in steel and its concentration. The concentration and effective diffusion coefficient values obtained were compared with those obtained in studies conducted on other API 5L steels. The comparison showed that the values obtained are consistent with those reported in the literature for API 5L steels.

Keywords: Green Hydrogen; Permeation; Electrochemistry; API 5L grade B; Hydrogen Embrittlement; Effective Diffusion Coefficient; Lattice Diffusion Coefficient.

This page was intentionally left blank.

Acknowledgements

Once up on a time, Sir Isaac Newton wrote a letter to the fellow scientist Robert Hooke saying: “If I have seen further, it is by standing on the shoulders of giants”. We all have our giants and they come and go in different times and spaces in our lives. Every major accomplishment in our lives is never a solo act, it is a consequence of all the giants that carried and taught us.

I want to thank to my mother for believing in me and for all the support in this rollercoaster, and all the rollercoasters I came across in my life, her support was vital, and my accomplishments are always hers too. To my brother that inspired me to follow the path of hard work, and for all the times he explained to my young self how to do simple math. To my father, I believe you are somewhere watching my accomplishments and hope you are proud of my efforts to follow my dreams.

To professor Carlos Fonseca, that had all the patience in the numerous times I asked for help and motivated me in this field that I now understand in a completely different way. Some teachers can really shape the path of their student. Thank you.

To doctor Omid Emadinia and INEGI, for all the help and sympathy during my project. I learned a lot from the professionals that I worked with a special thanks to doctor Malcher for the help with MatLab.

To my girlfriend Maryline for all the motivation and understanding, and for just being there to share the good and the bad.

To my friends that were always side by side with me during my university years, with a special mention to Diogo Amorim, João Morgado, Tiago Rodrigo and Afonso Maria.

This page was intentionally left blank.

Institutional Acknowledgements

I am grateful to INEGI for the opportunity to develop this project and all the help given during my thesis. Without this institutional support this work would not be possible.

I acknowledge the department of Metallurgy and Materials at the Faculty of Engineering of University of Porto, for all the lab resources made available and the professionals that I had the pleasure to share the laboratory with.

This page was intentionally left blank.

Contents

1.Introduction

1.1. Framework and Motivation

In the present moment, a transition from fossil fuels to renewable energies is taking place. Green hydrogen is taking a big role in this process, presenting a clean and versatile ways of transporting and producing energy.

One of the big questions around hydrogen is the way it is transported. Hydrogen can be transported and stored in reservoirs or tanks with the dangers and costs associated with that solution, giving rise to a new approach to address the problem. In a new approach, it was proposed that hydrogen can be transported in the existing natural gas pipelines, safely and with a lower associated cost. This solution has its own challenges, since gas pipelines are mainly made of steel, a material that is permeable to hydrogen and subject to hydrogen embrittlement.

In the Portuguese context, it is already implemented a natural gas pipeline grid where the API 5L grade B is present. It is of great interest to study how hydrogen permeates into this steel and the amount of hydrogen that is retained inside of the material lattice.

1.2. Objectives

In this work we aim to study the permeability of API 5L grade B steel to hydrogen. The main goal of the project, is to employ the electrochemical technique described in the ASTM G148-97, creating a procedure to charge the steel with hydrogen, and measure the diffusion coefficient and the hydrogen concentration inside the steel.

1.3. Hydrogen

1.3.1. Hydrogen Economy

In the present moment, the biggest quota of energy produced at a global scale comes from fossil fuels, a non-renewable source. This raises concerns about availability of the resources, environmental impacts and limitations related to policies adopted by the governments. It is not expected that an energy transition could occur, suddenly, in the next years. Instead, the transition for cleaner energy sources will happen as the technology develops in that area [1].

The expression “alternative energy sources” refers to sources of energy that don not depend on fossil fuels, being fossil fuels a primary source of energy nowadays. In this

definition, nuclear energy fits the group, although not all authors will consider nuclear energy as an alternative energy source given the risks and waste [1].

The use of renewable energies is increasing in the recent years due to the environmental concerns and the recent energy crisis. The sources for renewable energies can be divided in wind, solar, hydro, biomass, geothermal and ocean energy. The use of this kind of sources in energy production increased 4 times in the last decade, exceeding 20% of the global energy produced in 2018. The transition for clean sources of energy will have a major impact in the greenhouse gas emissions and will rise the research and development of new technologies [1].

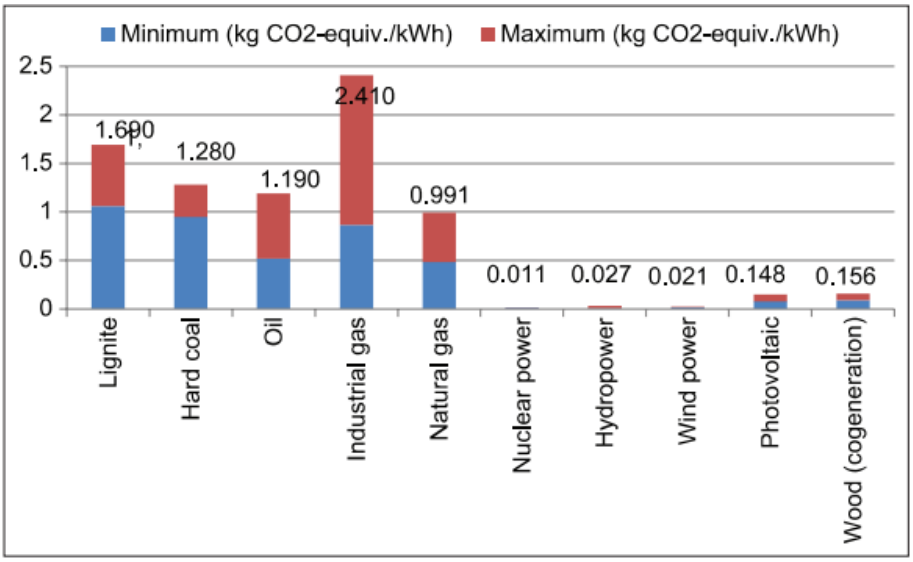

Graph 1: Greenhouse gas emissions during the entire life cycle of a power plant [1].

1.3.2. Hydrogen as a Renewable Energy Source

Following the trend to develop new technologies in the renewable energies field, hydrogen was posed as an option to fill the gaps. Unlike other renewable energy sources, hydrogen can tackle a wide range of concerns in this area. It poses as a safe, available, flexible and cost-effective way to bridge between the electricity production, industry and mobility sectors. Being cost effective is a debatable aspect of the hydrogen use as a source of energy since it is still not the best economical source of energy, although is a very promising technology that is improving very fast and is estimated to be more and more cheap as the technology evolves [2].

There are a couple of pilot projects that use hydrogen as a mean of storage and distribution of energy. Green hydrogen, that will be detailed in the next section, is the type of hydrogen on which these projects are based on. Currently, hydrogen fuel cells are being developed for an effective conversion of hydrogen into electricity. In the production of hydrogen technologies are being refined to use water as a source of hydrogen in a large scale and distribution and charging systems are being developed worldwide. The development of such technologies prove that hydrogen can be part of an integrated system

with other renewable energy sources filling the role of storing and transport of energy [2]. In figure 1, it is shown a scheme of the Utsira plant system.

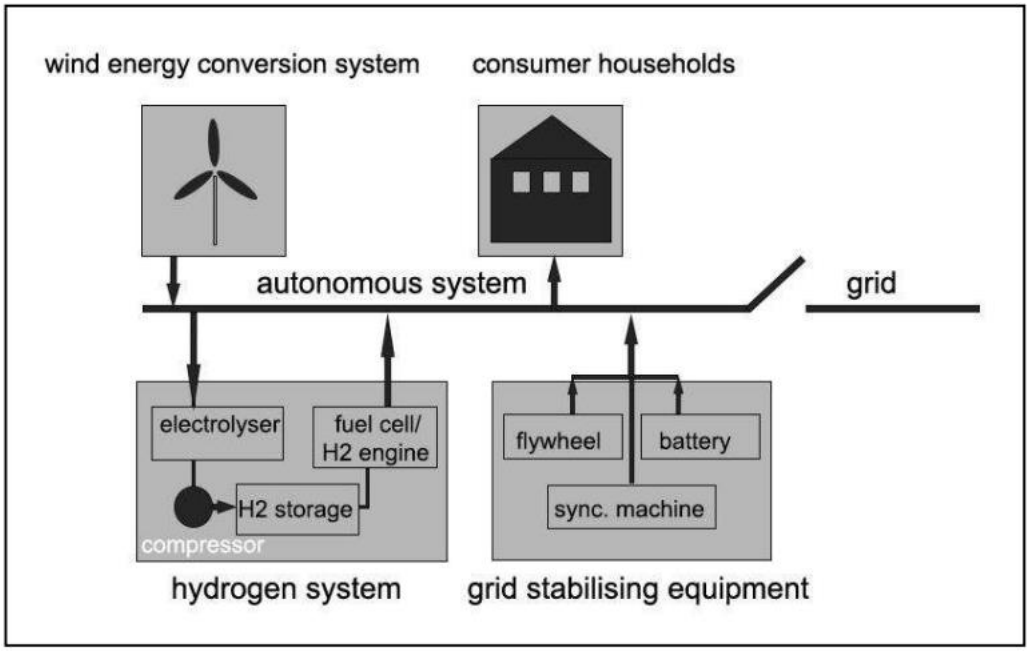

Figure 1: Utsira wind/hydrogen demonstration plant system schedule [2].

1.3.3. Hydrogen Production and Uses

Hydrogen is an energetic vector that can replace fossil fuels. The production of hydrogen can take many ways being the production of greenhouse gas emissions a concern in the process of obtaining hydrogen. Currently, the most common way to obtain hydrogen is by from the natural gas, a way that is associated with the emission of CO_2 gas. The method of obtaining hydrogen using water as the source via electrolysis, in itself, is the only clean way, on a macroscale, of obtaining hydrogen, although this process relies on electricity. This electricity can be obtained by coupling other renewable energy sources to the system, such as wind turbines [3].

Hydrogen is classified in a colour system, as shown in figure 2. This classification system allows to differentiate the hydrogen based on the production method employed and the emissions associated. Gray hydrogen is the most common kind of hydrogen in production nowadays. This type of hydrogen, like the blue hydrogen, is produced from natural gas. The difference between those two types is the fact that the first is produced

without a recapture of the greenhouse gases emitted in the process, contributing to arm of the environment and global heating [4].

On the other hand, green hydrogen, produced by water electrolysis, if coupled in a system with a renewable source of electricity will produce water and oxygen as a waste product. This way, the production and use of green hydrogen does not contribute to the emission of greenhouse gases, but still, it is an expensive process in the current days [4].

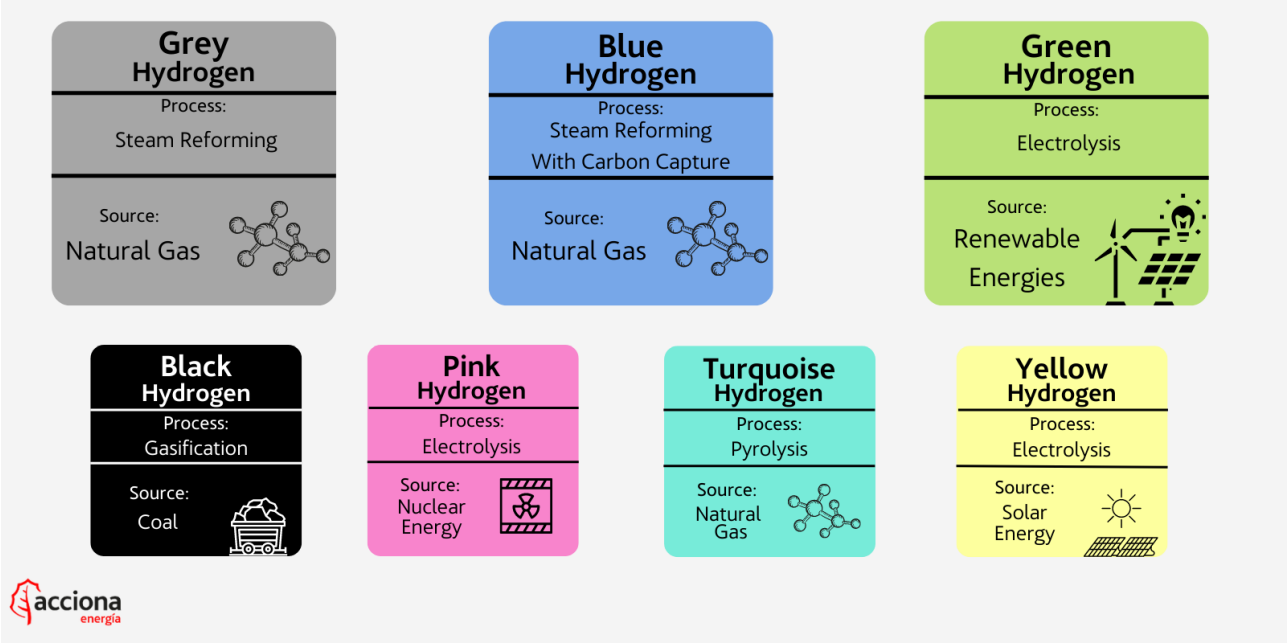

Figure 2: Hydrogen colour classification by source and process [5].

1.3.4. Plan of Action

In 2015, United Nations Organization defined the milestones and strategies for the reduction of greenhouse gas emissions. In that same year, the Paris agreement was signed, where a commitment for an energetic transition was established between the member nations, with the aim of slowing down the scaling of the global warming that, at the time, was in pace that would risk the environmental stability of the planet to an irreversible point [6].

As an answer to the climate question, and in the sequence of the Paris agreement, the European Union developed strategies to reduce the emissions of greenhouse gases. In that sense, in the year of 2020, a strategy for the use of green hydrogen as an energy vector was developed [7].

Following these strategies, feasibility studies on transport and storage of hydrogen were conducted. These works suggest that the existing natural gas pipelines could be a cost-effective way to transport hydrogen for long distances. A mix of natural gas and

hydrogen could go through the pipelines that would be subject to new operational conditions. Recent studies on the interaction between the natural gas/hydrogen mix and the steel show that the metal exposure to this fluid can lead to accelerated fatigue cracking, decrease in fracture resistance and reduced ductility and strength [8].

2. Literature Review

2.1. Hydrogen embrittlement

The transportation of hydrogen from the production plants to the consumption sites relies on transportation tanks or pipeline structures that are usually made of steel. This material is prone to a very well-known process called hydrogen embrittlement.

In metals, the properties are often determined by the interstitial atoms present in the microstructure. This topic is subject of study for a very long time and it was established that in the presence of second phases, lattice distortions and deformations, hydrogen can get trapped inside the material and the embrittlement effect can be noticed. The mechanisms of hydrogen trapping inside a steel are studied and it was found that in the special locations where hydrogen gets trapped different mechanisms of trapping can occur with different impacts in the hydrogen related failure [9].

It is generally accepted that hydrogen can compromise the properties of steel such as tensile strength, fatigue strength and fracture toughness. Due to the small size of the hydrogen atom, it is easy to penetrate the steel structure in the atomic form. This hydrogen is usually sourced to the steel by electrochemical charging and corrosion reactions at the surface of the material. As an answer to this question a variety of coatings can be applied at the surface of the steel in order to prevent hydrogen absorption [10].

The hydrogen embrittlement can be divided in two types of damage: reversible and irreversible. In the first case, atoms migrate to potential cracking locations and then accumulate in such sites which leads to a delayed fracture. This can be fixed with a thermal treatment to release the trapped hydrogen. On the other hand, in the irreversible hydrogen embrittlement, hydrogen will combine with other atoms and hydrogen itself to form molecules at defect sites, in this case, a high hydrogen gas pressure will be developed locally, and hydrogen-induced cracking can occur [10].

2.2. API 5L Grade B Steels

Pipelines were always the preferred mean of transportation of gas and oil products. Currently, the length of such structures in place is around 1.18 million kilometres, representing the most cost-effective way to deliver these kinds of products from the production site, to the consumption areas. In the European Union, this pipeline structure has been of major importance in recent years, since it can be used to transport renewable energy that will play a big role in the energy transition and, at same time, allowed a quick change of gas suppliers since the sanction on Russia, one of the major gas producers in Europe. Due to the nature of hydrocarbons, these pipes are always subject to deterioration by corrosion and mechanical damage. That said, it is important to study the behaviour of

the pipe materials in service in order to understand the capabilities and safety status of the grid over the time [11].

The API (American Petroleum Institute) 5l standard was developed to set the standards for the fabrication and requirements in steel pipes that are used in gas and oil transportation. The tubes produced for such applications must be wide and with great mechanical strength. During operation, the walls with reduced thickness should support high pressures, which results in higher productivity and economic benefits, during construction. These pipes are made of carbon steel and their series specifies the mechanical strength. There are three main series in the API 5L standard: A, B and X. The X series represents steels with higher mechanical strength. Besides this, there are two levels of specification to produce these pipes: PSL 1 and PSL 2. Those levels refer to the degree of accordance with the standard requirements [12].

The API 5L grade B steel is a low carbon steel with a ferrite and pearlite microstructure, as shown in figure 3 [13].

Table 1: Chemical composition of API 5L grade B [13].

C %	Mn %	P %	S %	Others %
0.28	1.2	0.03	0.03	0.15

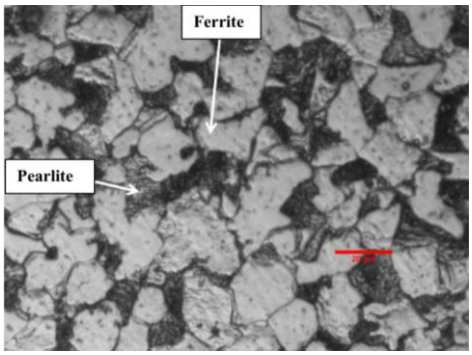

Figure 3: Microstructure of API 5L grade B (Ferrite and Pearlite microstructure) [13].

Being a carbon steel, the API 5L grade B, in the right conditions, like cathodic charging or gas corrosion, is prone to hydrogen diffusion inside the structure. The diffusivity of the hydrogen and the amount that gets trapped inside the steel is a function of several variables, being the chemical composition, the microstructure and defects present, the major ones. It is well known that hydrogen trapping inside a steel, induce hydrogen embrittlement and hydrogen induced cracking (HIC). Steels with higher carbon content are more prone to HIC. Studies show that pearlite and martensite/austenite phases can increase the hydrogen trapping in steel microstructures, while softer structures

like ferrite do not show this effect. Microstructures like ferrite and bainite are more resistant to HIC than the ones containing ferrite and martensite [14].

Table 2: Comparison between different API 5L steel grades, in terms of mechanical strength, hydrogen diffusion coefficient, microstructure and carbon content and subsurface hydrogen concentration after hydrogen charging (F-ferrite; B-bainite; P-Pearlite) [14].

Material	Microstructure	Carbon Content (%)	Min. Yield Strength (MPA)	Diffusion Coefficient (cm^2/s)	Subsurface Hydrogen Concentration (mol/cm^3)
API 5L X-52	F+B	<0.1	360	$10.3\ 10^{-6}$	$2.94\ 10^{-6}$
API 5L X-70	F+B	<0.1	485	$11.2\ 10^{-6}$	$3.15\ 10^{-6}$
API 5L X60	F+P	>0.1	415	$5.02\ 10^{-6}$	$4.65\ 10^{-6}$
API 5L X-65	F+P	>0.1	450	$6.31\ 10^{-6}$	$4.36\ 10^{-6}$

2.3. Hydrogen Trapping and Diffusion in Pipeline Steels

When in service, steel contacts with several hydrogen sources. Corrosion is one of the hydrogen sources in steel surfaces. In alkaline or neutral environments, the metal reacts with the solution and hydrogen is adsorbed at the metal surface (M) as shown in the following equation 1:

$$H_2O + M^+e \leftrightarrow MH_{ads} + OH^- \quad (1)$$

After the adsorption, hydrogen can be desorbed back into the medium or enter the metal following an equilibrium equation, as described in eq. 2:

$$MH_{ads} \leftrightarrow MH_{abs} \quad (2)$$

Combined with applied stress, the absorbed hydrogen can get trapped in the steel microstructure and cause hydrogen embrittlement [15].

Oil and gas pipelines are often under cathodic protection to avoid corrosion in the external side of the pipe. In this process, the cathodic potential imposed on the steel will promote a spontaneous hydrogen reduction in the surface of the material [16].

Trapped hydrogen can degrade the structural integrity of steel promoting hydrogen induced cracking. This issue has been pointed as the leading failure cause in energy and pipeline industry [15;17].

The trapping process starts with the entry of hydrogen at the steel surface. The atomic hydrogen that enters the steel diffuses inside the structure and can be trapped in locations called trapping sites. Traps can be reversible, if the binding energy is low, or irreversible, if the binding energy is higher. Microstructural sites such as dislocations, low-angle grain boundaries, coherent precipitates and twin boundaries are examples of reversible traps. On the other hand, carbide interfaces, incoherent precipitates and high angle grain boundaries [15;17].

The hydrogen trapped in reversible sites is called diffusible hydrogen. In these locations hydrogen will get trapped and detrapped until an equilibrium is reached. In irreversible sites, hydrogen will be trapped permanently and will not be released in normal conditions [15].

The concentration of hydrogen immediately beneath the material surface (subsurface) characterizes the efficiency of the hydrogen permeation. The permeation is controlled by the diffusion coefficient (D_{eff}). These parameters are essential to characterize the hydrogen uptake, transport and permeation in metals [18].

2.4. Hydrogen Permeation Technique

There are many experimental procedures for the evaluation of hydrogen-metal interactions. In order to determine the total amount of hydrogen in a sample, inert gas fusion methods are often used. On the other hand, barnacle cell methods resort on electrochemical charging to evaluate the amount of diffusible hydrogen in a metal [8].

Studying the effect of hydrogen diffusion and trapping in the mechanical properties of steel is not a simple process and requires a permeation technique to introduce hydrogen atoms inside the material [15]. In figure 4, it is shown a scheme of the process. The permeation process itself is complex but can be divided in several successive stages [19]:

1. Adsorption and absorption at the steel surface;
2. Diffusion through the membrane;
3. Desorption;

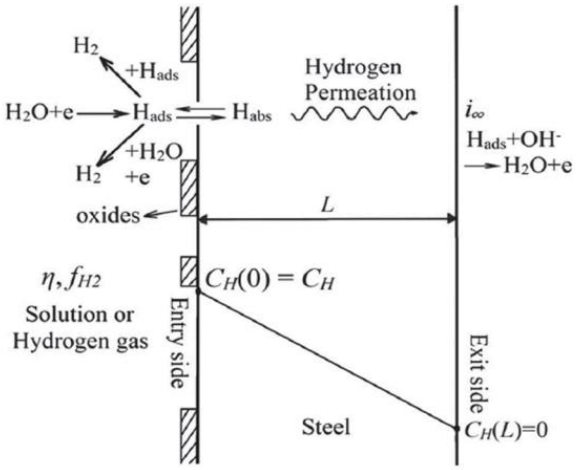

Figure 4: Schematics of hydrogen permeation in metals [18].

Each one of these stages can be characterized as a resistance to the entry of hydrogen in the steel. That said, we have three resistances: resistance to the entry of hydrogen (R1), resistance to the diffusion of hydrogen (R2) and resistance to the exit of hydrogen (R3). The experimental conditions must be in a way that ensures that the resistance to the diffusion of hydrogen is bigger than the other two by orders of magnitude (R2>>R1 and R3). The resistance to hydrogen diffusion in a metal is given by the division of the thickness of the membrane by the diffusion coefficient (R2=L/D). One way to ensure that R2 is the leading resistance is to have thicker specimens. The hydrogen flux is proportional to the inverted sum of the resistances as follows [19]:

$$J_\infty \alpha \frac{1}{(R_1 + R_2 + R_3)} \quad (3)$$

The electrochemical permeation technique allows to introduce hydrogen atoms inside the steel by cathodic charging and, at same time, evaluate the amount of atoms that leave the metal surface. This technique was first described by Devanathan and Stachursky [15].

The ASTM G148-97 is a standard, based on the electrochemical technique developed by Devanathan and Stachursky, that gives the procedure for the evaluation of hydrogen uptake, permeation and transport in metals. The experiment defines the test environment, apparatus, specimen, surface conditions and data analysis for the hydrogen electrochemical permeation [20].

The test is conducted on a dual chamber electrochemical cell that sandwiches a metal specimen of a certain thickness (L) in the middle, with a defined permeation area (A) exposed to both chambers. In one chamber, a cathodic current is imposed to form hydrogen in one side of the metal surface, that will permeate through the steel. In the

other chamber, a fixed potential is imposed to the metal in order to oxidize the hydrogen that passes from the charging side of the membrane to the *oxidation side*. The current that will be generated from the oxidation will be measured with a potentiostat and a graph of current *vs.* time will be recorded [17;20;21]. In figure 5, it is shown a scheme of the process.

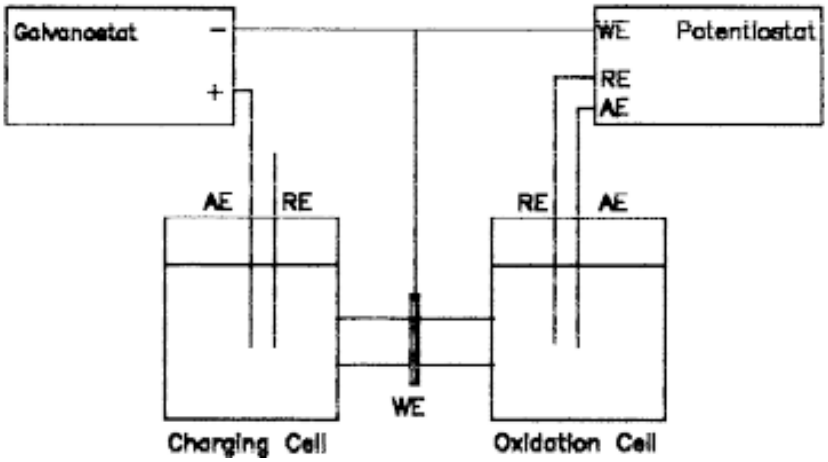

Figure 5: Cell Assembly and measuring apparatus [20].

In the graph two essential values will be obtained in each permeation, the initial steady state permeation current (i_p^0) and the final steady state permeation current (i_p^∞)[15].

2.4.1. Determination of the Diffusion Coefficient

During the electrochemical permeation the permeation transient versus time will be plotted. For the determination of the hydrogen diffusion coefficient three methods are known: the breakthrough time method, the time lag method, and the curve fitting to an approximate solution of the Fick's Law [8].

The breakthrough time (t_{bt}) is the time, from the beginning of the permeation until the current reaches 10% of the final steady state permeation current. Based on the breakthrough time the diffusion coefficient (D_{bt}) is determined as in equation 1 [8]:

$$D_{bt} = \frac{L^2}{15.3 t_{bt}} \tag{4}$$

Similarly, the lag time method relies on the time needed to reach 63% of the steady state current. From this, the diffusion coefficient (D_{lag}) can be calculated as in equation 2 [8]:

$$D_{lag} = \frac{L^2}{6t_{lag}} \tag{5}$$

Additionally, the diffusion coefficient (D) can be determined by fitting the entire permeation to an approximate solution to Fick's second law, using a least-squares regression, as shown in graph 2 [8].

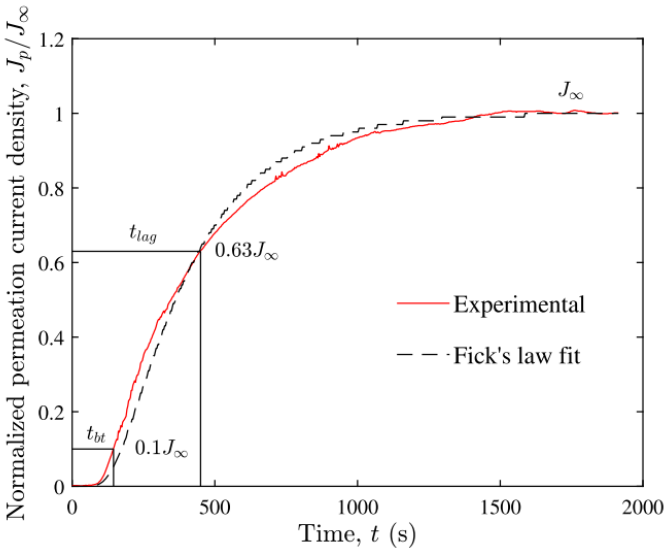

Graph 2: Typical rise permeation transient with all three methods represented [8].

The fitting equation assumes two different forms, one for rising transients and other for decaying transients as follows [15]:

$$i_n = \frac{i_p - i_p^0}{i_p^\infty - i_p^0} = \frac{2L}{\sqrt{\pi Dt}} \sum_{n=0}^{\infty} \exp\left(-\frac{(2n+1)^2 L^2}{4Dt}\right) \text{ (Rise transients)} \tag{6}$$

$$i_n = \frac{i_p - i_p^\infty}{i_p^0 - i_p^\infty} = 1 - \frac{2L}{\sqrt{\pi Dt}} \sum_{n=0}^{\infty} \exp\left(-\frac{(2n+1)^2 L^2}{4Dt}\right) \text{ (Decay transients)} \tag{7}$$

There are two types of diffusion coefficient, an effective one and a lattice one. The effective diffusion coefficient takes is determined in the presence of the trapping effect. The lattice diffusion takes place when all the traps are full and the hydrogen is flowing through the metallic lattice. [15]

2.4.2. Hydrogen Permeation Flux and Permeation Rate

The permeation flux can be measured from the steady state permeation current, and gives the amount of hydrogen per unit of area per time [17]:

$$J_H = \frac{i_p^\infty}{nF} \, (mol\ H/m^2\ s) \tag{8}$$

The permeation rate is the amount of hydrogen that passes through the thickness of a sample per unit of length, per unit of time [17]:

$$J_H L = \frac{i_p^\infty}{nF} L \, (mol\ H/m\ s) \tag{9}$$

2.4.3. Hydrogen Sub-surface Concentration

The solubility of hydrogen in a metal can be measured having the effective diffusion coefficient and the permeation rate. From that stage the apparent hydrogen concentration in the subsurface of the metal is given by the following equation [17]:

$$C_{app} = \frac{J_H L}{D_{eff}} \tag{10}$$

2.5. Superficial Conditioning and noise reduction

In the electrochemical permeation process, the superficial condition of the steel membrane will have a major impact in the transients obtained. In the ASTM G148-97 standard, a procedure is given to mitigate the effects of superficial roughness, presence and development of oxides, and noise in the permeation readings.

It is recommended to perform a sequence of polishing, cleaning, and coating process, in the steel sample. The coating process can be applied only to the oxidation surface, depending on the objectives and material of the experiment. For hydrogen permeation, there are two coatings that are suitable for the oxidation side of the membrane: palladium or nickel [20].

Since steel is an active metal, when the coating is not applied, the oxides formed during polishing and the time before charging (e.g. when obtaining a background current before the permeation starts) will retard the hydrogen entry in the metal. Plus, reduction of oxides occurs when a potential is applied, which occurs before and during the permeation process. The results that are obtained when dealing with an uncoated oxidation surface maybe not be consistent with the models in study [18]. That said, not only the coating is essential but also the process and material are choices are relevant.

Studies show that, in uncoated membranes, the rougher the surface condition is, the more the cathodic current of hydrogen evolution increases. At the same time there is

less hydrogen absorption in the interior of the metal. Some microstructural defects that happen in the surface of the metal when the preparation leads to a rougher surface, it can increase the catalytic reaction of atomic hydrogen recombination [19].

2.6. Coatings

2.6.1. Electroplating

The process of electroplating intends to deposit a layer of metal upon a substrate by electrodeposition. This method is characterized by passing an electric current between two electrodes that must be immersed in a conducting substance, charged with ions (electrolyte). An electrical potential must be applied between the two electrodes, usually by connecting to a power supply, to promote the dislocation of ions. Positively charged ions will move to the cathode while the negative ones flow to the anode. This movement of ions will promote electron exchanges at the surface of the electrodes, resulting in a movement of electrons that will close the circuit [22].

2.6.2. Rate of Deposition

Michael Faraday studies on electrodeposition show that there is a proportional relationship between the amount of metal deposited at the surface of the cathode and the energy applied to the system. That said, the thickness of the metal layer deposited at the cathode is determined by the current and time sourced during the plating process [22].

2.6.3. Nickel Electroplating

Assuming a current efficiency of 100%, the mass deposited at the cathode can be determined by equation 1, for nickel. In this equation, I is the current (in amperes), t is the time (in seconds) and W is the weight of nickel deposited at the surface (in grams) [22]:

$$W = 1.095\, lt \tag{11}$$

The current efficiency at the cathode will depend on the platting solution and usually varies from 90% to 97%. A value of 95.5% is usually applied. The anode efficiency is assumed to be 100% if the experimental conditions are maintained properly in normal ranges, such as pH and chloride levels [22]. In figure 6, it is shown a scheme of the process.

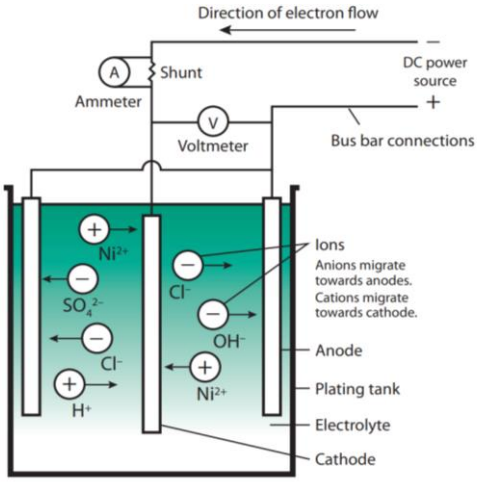

Figure 6: schematic of the nickel electroplating process [22].

2.6.4. Average Thickness of the Nickel Coating

The average thickness of the coating, T (in μm), can be estimated by equation 1, where I is the current applied, t is the time (in seconds) and A is the surface area (in dm^2).

$$T = \frac{12.294\ \mathrm{It}}{\mathrm{A}} \tag{12}$$

The current density is given by the ratio of I/A and is 100% if the equation is applied as stated. It is known that the current efficiency is not 100% as shown before which means that proper adaptations should be taken into account if the tolerances of the thickness are in a very small range.

The shape of the piece to be platted will influence the local thickness of the layer. The equations stated before give the average thickness and this thickness will vary depending on the distance between the surface of the piece and the anodes, the shape and the superficial roughness of the cathode. The distance from the anode must be the same for any point of the piece and the current distribution should be even. To achieve a thin and even layer of nickel on the plated surface, ideally, the cathode should be in a regular format (cylinder or sheet) and the surface must be flat and smooth, this will ensure an uniform distribution of the current [22]. In figure 7, it is shown a scheme of the process.

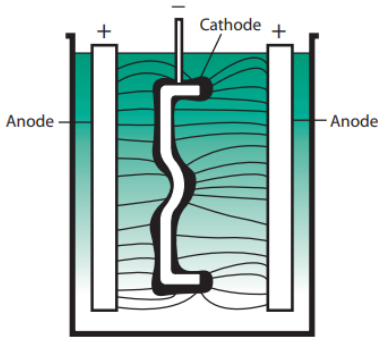

Figure 7: Non-uniform distribution of the current and the resulting thickness variation [22].

2.6.5. Chemistry of Deposition

In 1916, Oliver Watts formulated a solution for an electrolyte combining nickel sulphate, nickel chloride and boric acid. This solution can be used in multiple operating conditions and varying component ratios in order to achieve different platting results. Usually, this electrolyte is used at temperatures that range between 40 to 60 ºC and acidic pH values. In Watts solution each ingredient as a different role. The nickel sulphate will act as a primary source of nickel ions. On the other hand, nickel chloride will fill two roles: will improve the conductivity of the solution and, at same time, will help in the dissolution of nickel anodes. The last ingredient on the list is boric acid, this ingredient plays the role of maintaining the pH of the solution. The pH of the solution as a tendency to increase due to the inefficiency of the cathode which results in the formation of H^+, that will be minimized as the boric acid forms ions to replace the lost hydrogen [22].

New studies were able to obtain excellent results at ambient temperature. This fact is of particular importance in metals where high temperatures can be detrimental for the final properties of the substrate. Those studies revealed that the optimal current to be applied in thin nickel coatings would be somewhere between 10 and 50 mA/cm^2. The Watts electrolyte used was a mix of 77% nickel sulphate, 13% nickel boride and 10% boric acid. Agitation is another factor that plays an important role on the plating process, it should be mild to ensure an even concentration of the electrolyte during the whole process. Another key factor prior to the platting of the substrate was the surface conditioning that involved grinding and polishing procedures alternated with ultrasonic baths for a superior surface finish free from scratches and grease [23].

2.6.6. Influence of the Nickel Layer on Hydrogen Permeation

When permeating coated metal samples with the main goal of studying the permeation of the substrate, it is important to guarantee that the homogeneity of the material. That said, the electrochemical permeation technique is usually performed on coated steel assuming that the coating will not influence the permeation outcome [24].

In order to understand the influence of the nickel layer in a steel substrate, during hydrogen permeation, studies were performed with varying thicknesses of nickel layers in steel samples. Those studies found that as the thickness of the nickel layer increases, the diffusion of hydrogen decreases. This is attributed to the decrease of hydrogen diffusivity in the nickel [24]. In graph 3, it is shown the comparison of the current densities achieved using different thicknesses of nickel coating.

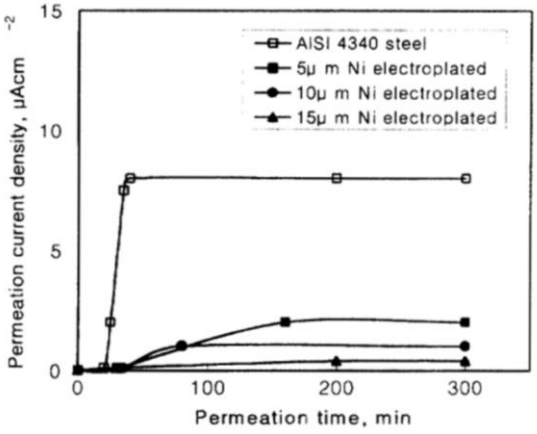

Graph 3: Permeation current density over time for different thicknesses of nickel coating in AISI 4340 steel [24].

3. Materials and Methods

3.1. Sampling

3.1.1. Material

In this laboratory analysis, the "API 5L grade B" steel, provided by the company "Portgás," was employed. This material was sourced from pipelines utilized in the conveyance of natural gas, undergoing cutting and grinding procedures to yield flat plates of diminished thickness.

In table 3, the chemical composition of the steel is presented. On the microstructural analysis ferrite and pearlite grains were observed. The chemical etching with Nital 2% revealed brighter equiaxial ferrite grains and darker pearlite grains, as shown in figure 8.

Table 3: Chemical composition of the steel (source: internal report)

Chemical Composition (wt%)														
C	Si	Mn	P	S	Cr	Mo	Ni	Al	Cu	Ti	V	W	Pb	Fe
0.14	0.21	0.66	0.02	0.006	0.05	0.03	0.11	0.03	0.19	0.003	0.003	-	-	Rem.

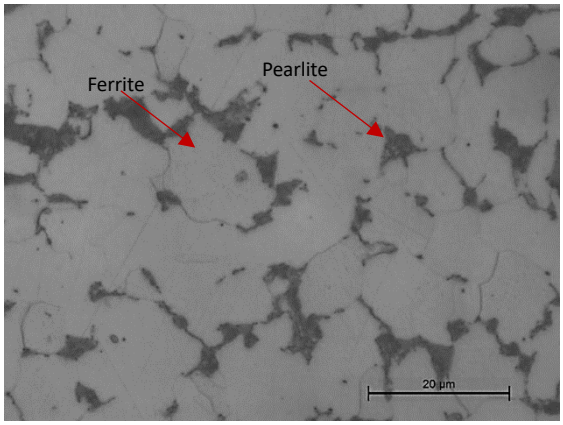

Figure 8: Microstructural analysis of API 5L grade B sample etched in 2% Nital solution.

3.1.2. Sample Preparation

In an initial phase, all specimens underwent a grinding process. The purpose of this procedure was the elimination of superficial defects, such as grinding marks and corrosion, ensuring a flat surface devoid of oxides.

The grinding was carried out using a Struers RotoPol rotary polishing machine, progressing through abrasives of 120 grit, 180 grit, 300 grit, 500 grit, and 1000 grit. Subsequently, only the specimens designated for metallographic analysis underwent an additional grinding step utilizing a 2500 grit abrasive, followed by polishing on 6 µm and 1 µm cloth pads utilizing diamond suspensions of matching particle size.

Between each grinding and polishing stage, the specimens were immersed in a solution of ethanol (98%) within an ultrasonic bath, aimed at the removal of any residues originating from the preceding step.

Upon conclusion of this procedure, the specimens were marked, and a useful area was demarcated on both sides of the sample, the dimensions of which were duly recorded.

3.2. Microstructural Analysis

3.2.1. Chemical Etching

To differentiate the distinct phases and metallic inclusions within the material, a chemical etching process was conducted employing a 2% Nital solution. This method was applied to the samples prior to optical microscope analysis, facilitating the delineation of ferritic grain boundaries and affording a pronounced contrast between this variety of grain and the perlite grain.

This approach enabled the clear visualization and differentiation of these microstructural constituents, enhancing the characterization of the material's internal composition and architecture.

3.2.2. Microscopic Examination under Optical Microscopy

Microscopic Examination Utilizing Optical Microscopy was conducted with the assistance of the Leica Lens X equipment. Leveraging both Leica X software and ImageJ, a thorough investigation of microstructural attributes was facilitated, alongside the precise measurement of sample thickness.

The determination of sample thickness was achieved by computing the mean of measurements taken across the transverse section of each permeated specimen. This approach not only allowed for comprehensive microstructural analysis but also yielded accurate thickness quantification, contributing to a comprehensive understanding of the material's properties.

3.3. Sample Coating

3.3.1. Cleaning

Prior to commencing the coating process, the samples underwent a cleaning procedure aimed at degreasing and removing particles resulting from preceding steps. This protocol unfolded in three distinct phases:

1. Detergent Cleaning:

The first phase entailed a cleaning regimen involving a detergent solution. The laboratory-prepared detergent comprised a mixture of 24 g of LSS (sodium lauryl ether sulfate), 1 g of NaOH (sodium hydroxide), and 100 ml of water. This amalgamation was stirred using a magnetic stirrer until an immaculate, fully dissolved solution was achieved. Subsequently, the samples were immersed in this detergent solution and agitated within a goblet, facilitating the cleansing of their surface.

2. Detergent Removal:

For the second phase, the samples were submerged in a goblet containing warm water and agitated to eliminate any residual traces of detergent and superficial grease.

3. Ethanol Cleaning:

Lastly, the samples were immersed in 98% ethanol, serving the dual purpose of preserving the sample for subsequent steps and ensuring effective drying between procedures without inducing corrosion.

By rigorously adhering to this multistage cleaning process, as shown in figure 9, the samples were rendered free of contaminants, ensuring the pristine condition necessary for the subsequent coating procedure.

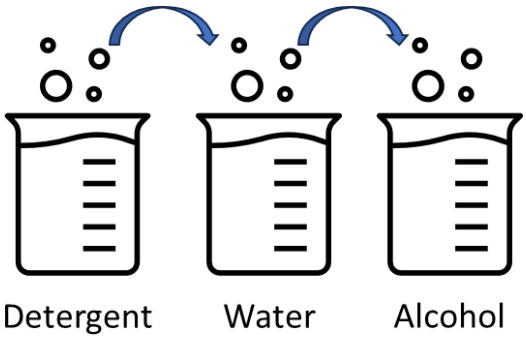

Figure 9: Cleaning process of the samples.

3.3.2. Nickel Coating

The nickel coating was accomplished through an electroplating process employing a Watts solution formulated within the laboratory setting. This technique facilitates the determination of the deposited layer's thickness by controlling both time and the applied current during the process.

The Watts solution was prepared by amalgamating 75 grams of nickel sulphate, 12.5 grams of nickel chloride, and 10 grams of boric acid within 250 millilitres of water.

In the electroplating procedure, two nickel anodes were employed, connected to the positive terminal of a power supply. The steel sample (substrate), serving as the cathode, was connected to the negative terminal of the power supply.

This method of electrodeposition allows for the controlled deposition of nickel onto the substrate, enabling the modulation of coating thickness based on precise adjustments of time and current parameters. By employing this electroplating technique, a uniform and well-defined nickel coating was achieved, endowed with a thickness proportionate to the specified process parameters. The setup for the coating is shown in figure 10.

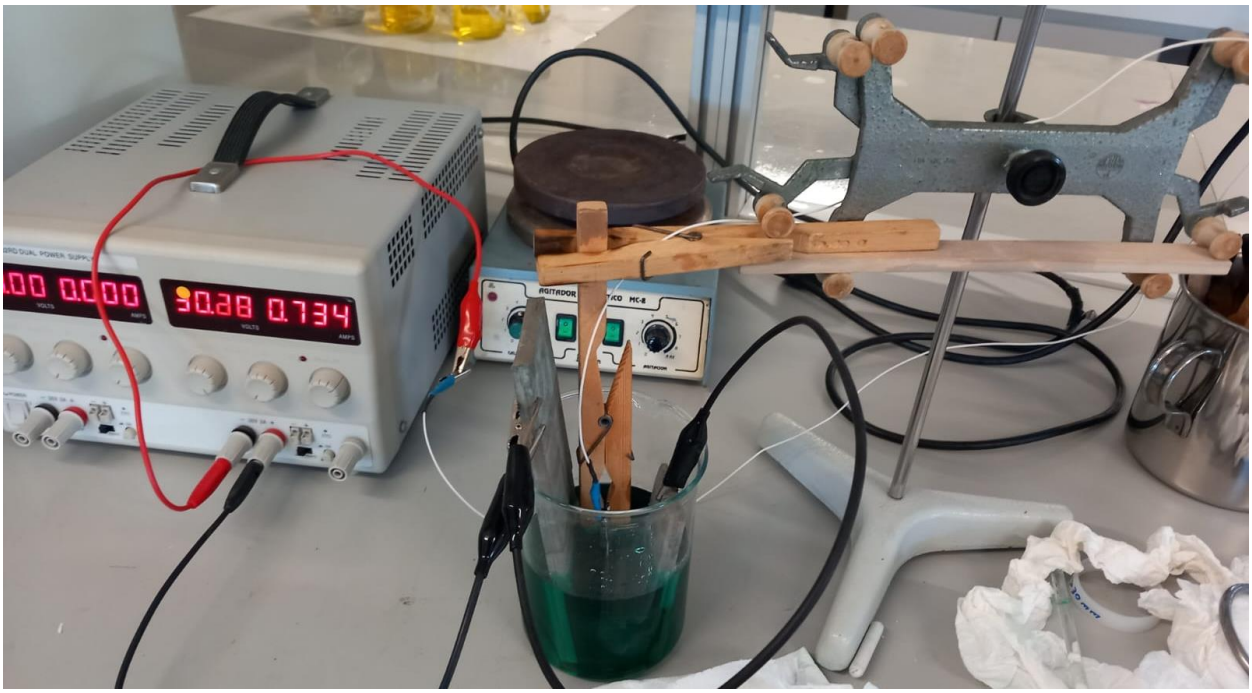

Figure 10: Nickel coating setup.

In order to achieve a nickel layer with a thickness of 50 nm across the entire useful area of the sample, a current density of 3 A/dm^2 was applied for a duration of 4.9 seconds. It is imperative that the solution remains in continuous agitation during the procedure to facilitate the deposition of nickel ions onto the substrate.

Upon the successful attainment of the coating, the sample is subjected to a cleansing process involving distilled water. Subsequently, one side of the sample undergoes a polishing procedure, specifically targeting the removal of the coating from the surface corresponding to the hydrogen loading side. Following this, the sample is immersed in a bath of 98% ethanol within an ultrasonic machine. Finally, the sample is dried utilizing compressed air.

This sequence of post-coating steps ensures the thorough and precise treatment of the specimen, culminating in the removal of excess coating material from one side while maintaining the integrity of the coating on the opposite side. The utilization of ultrasonic cleaning and compressed air drying guarantees the removal of residual impurities and the preservation of the coated sample's structural and compositional integrity.

3.4. Data Retrieving and Permeation

3.4.1. Permeation Cell

The permeation cell has been ingeniously designed in the configuration of two half-cells, with one facet dedicated to hydrogen charging ("Red") and the other to detection ("Ox"). The sample is positioned between these two half-cells, delineating a permeation area confined by a pair of O-rings, each encompassing an area of 4.52 cm^2.

On the detection side ("Ox"), a mercury reference electrode containing a potassium hydroxide solution, procured from Gamry Instruments, is introduced. Accompanying this reference electrode are a platinum counter electrode and an inlet for inert gas (nitrogen). These electrodes, alongside the test sample, are linked to a Gamry Instruments potentiostat (PARSAT I-1010).

Conversely, on the charging side ("Red"), a platinum electrode is installed, connected to the positive pole of a power source. Simultaneously, the test sample is linked to the negative pole of the same power supply.

Both sides of the permeation cell are replete with a 0.1 M sodium hydroxide solution, ensuring an appropriate electrochemical environment for the permeation process.

This intricate arrangement of half-cells, electrodes, and electrolytes establishes an environment conducive to hydrogen permeation studies, enabling precise control and monitoring of the permeation process. The diverse elements within the setup collectively contribute to accurate measurements and analysis of hydrogen permeation characteristics. A scheme of the used setup is shown in figure 11.

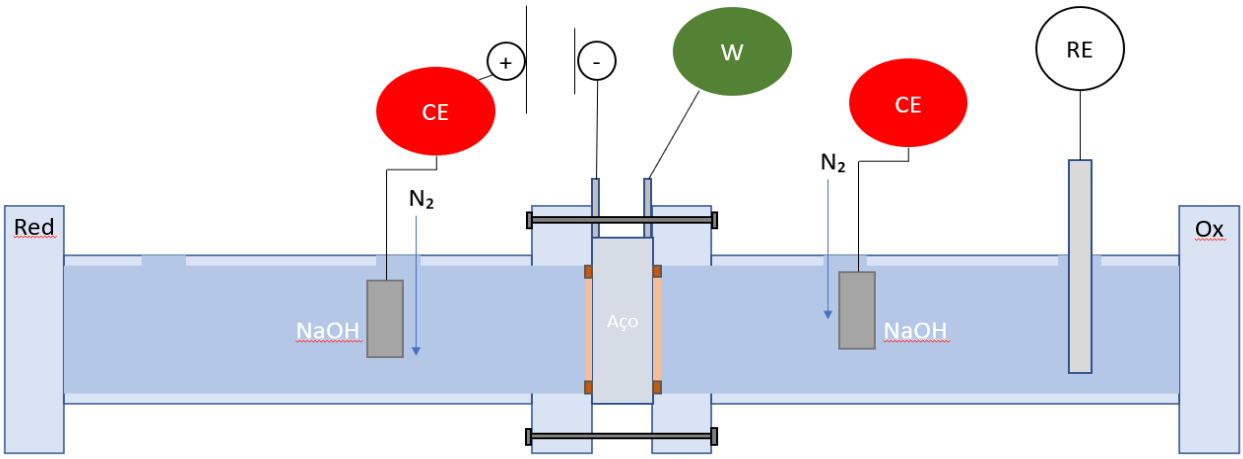

Figure 11: Schematics of the permeation cell.

3.4.2. Background Current

Prior to initiating the permeation process, it is imperative to acquire a background current on the detection side. To accomplish this, the "chronoamperometry" function is employed within the Gamry Instruments interface software. Within this operational mode, the ability to measure current over time is realized while maintaining the potential at a predetermined, pre-programmed value, as illustrated in figure 12.

This foundational step serves to establish a baseline current level for subsequent analyses and is pivotal for accurate data interpretation during the hydrogen permeation study. The chronoamperometric technique enables the systematic acquisition of current-time data, elucidating the electrochemical behaviour of the system under controlled conditions and facilitating the distinction of the hydrogen permeation signal from background noise.

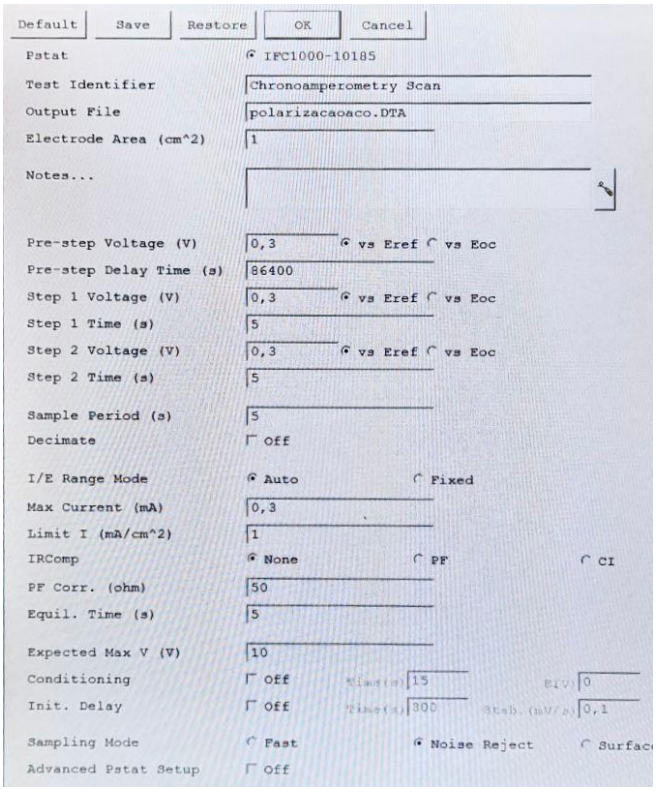

Figure 12: Procedure settings in the Gamry Instruments software.

The background current must attain a state of stability and remain below 0.2 μA/cm². Upon reaching this criterion, transition to the hydrogen charging phase is permissible, maintaining an unswerving record of current in relation to time. This diligent monitoring of the current-time relationship serves as a cornerstone in capturing the intricate dynamics of the hydrogen charging process.

3.4.3. Hydrogen Charging

Once a satisfactory background current level has been achieved, the progression to the permeation procedure becomes feasible. Within this process, initiation involves the imposition of a current density of 10 mA/cm^2 on the charging side until an elevation in current is observed on the detection side, eventually reaching a plateau of stability. In this initial permeation, the duration required to attain a state of stable current shall extend beyond 24 hours.

Following the completion of the inaugural permeation, subsequent increments and decrements of current on the charging side ensue, orchestrated to capture the profiles of permeation and stable plateaus over the course of time. These predetermined values of imposed current and the instances of charging current alteration are meticulously logged. During the culmination of the last transient response documented, the power supply is deactivated, resulting in the observation of the current descent until values akin to the background current are attained, thereby signifying the termination of the assay.

This systematic approach of iterative charging current modulation and data recording constitutes a comprehensive framework for elucidating the intricate phenomenon of hydrogen permeation, delineating the interplay between various factors and processes in the evolution of the material permeation behaviour.

4. Results and Discussion

4.1. As Received Samples

The received samples were taken from an existing pipeline in service. From the donor pipe, the steel was cut with a circular saw and rectified to achieve a rectangular shape and flat surface. The samples were used as received and did not receive any heat treatment to release tensions or release hydrogen introduced during service and sampling process. It is noticeable the small scratches left from the rectifying process at the time the samples were received. It was also noticeable, the high amount of oxide that is formed at the surface of the steel, when left exposed to the air. In figure 13, we can observe a sample before polishing.

Figure 13: Surface condition of the received samples.

The received samples had a significant bending angle that is noticeable in the polishing process. For that reason, the first polishing steps took a very long time and required a significant amount of force on the surface of the sample.

Between each polishing step it, when exposed to the air, the surface of the sample was readily oxidized. The deep scratches from the rectifying process were a privileged location for the formation of oxides and, as the surface went through the polishing sequence towards the mirror like superficial condition, the harder it would be to form oxides at the surface.

Previous studies found that the superficial roughness had a major impact in the deposition of nickel, which is expected to have greater influence in thinner coatings like the nanometric film that is supposed to be reproduced for the hydrogen permeation. The coating in scratched or bended surfaces will act as places of accumulation of nickel, producing a nonuniform deposition.

4.2. Thickness Measurements

The thickness measurements were performed before the coating process to avoid contamination and the formation of oxides in the uncoated surface.

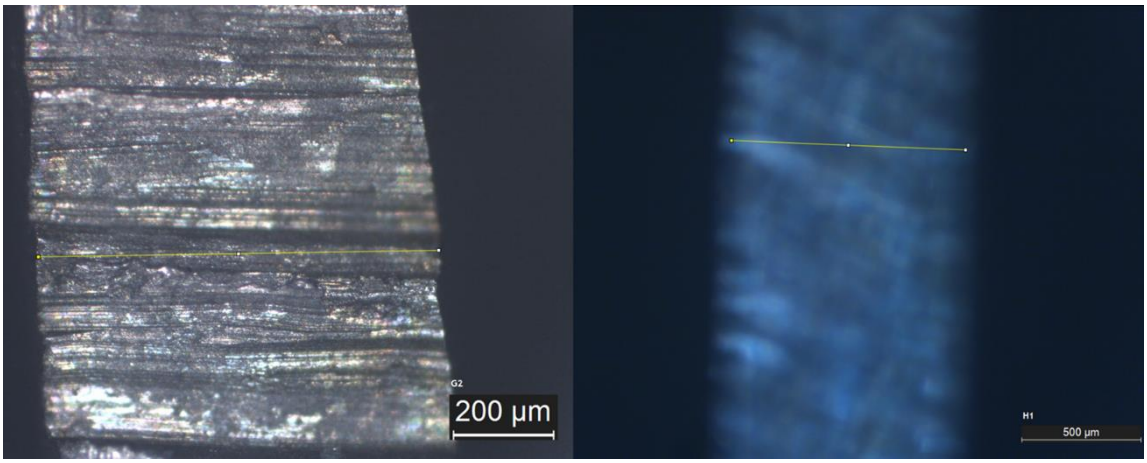

Figure 14: Thickness measurement using ImageJPro software.

Reoccurring to ImageJPro software, 5 longitudinal measures were taken from the samples G2 and H1, as shown in figure 14 and detailed in table 4. It was determined that the average thickness of the samples was 0.08 cm and 0.1 cm respectively.

Table 4: Thickness measurements of the samples.

Sample / Measurement	G2 (cm)	H1 (cm)
1	0.080	0.095
2	0.081	0.099
3	0.079	0.092
4	0.081	0.104
5	0.079	0.101
Average	0.080	0.100

The G2 sample showed an inferior thickness than expected. Previous works usually perform this experiment with thicker samples, usually over 0.1 cm. This is desirable if the aim of the work is to access the hydrogen diffusion in the cross section of the metal sample. When performed in thinner samples, this experiment can lead to false results. This occurs because of the influence of the surface condition and the coating layer on hydrogen diffusion. The thickness must be enough to ensure that the measured coefficients come from the metal itself. This effect is described in equation 3.

That said, at this point, the H1 sample achieved the minimum thickness that will ensure a good measurement.

4.3. Coated Layer

It was intended to test the effect of the coating in the permeation results. That said, the coating conditions were different for the two samples in this study. From equation 11, the average thickness was controlled varying the time of the deposition.

Table 5: Deposition conditions for samples H1 and G2.

Sample	I (A/dm^2)	A(dm^2)	t (s)	Thickness (μm)
H1	3	0.234	4.88	0.05
G2	3	0.232	40	0.41

Visually inspecting the surfaces of the two samples it is noticeable that the smoothest layer was achieved in the conditions employed for the H1 sample. The mirror like finish in this sample, contrasts with the rougher and foggy-like finish of G2. Some oxidation can be noticed in figure 15 for both samples, this is due to the stage at which the image was captured. The figure was obtained after the permeation. Previous images could not be obtained without risking oxide formation between the cleaning step and the beginning of the permeation. The transition between those steps must occur as fast as possible to avoid contamination and oxide formation at the surface layers.

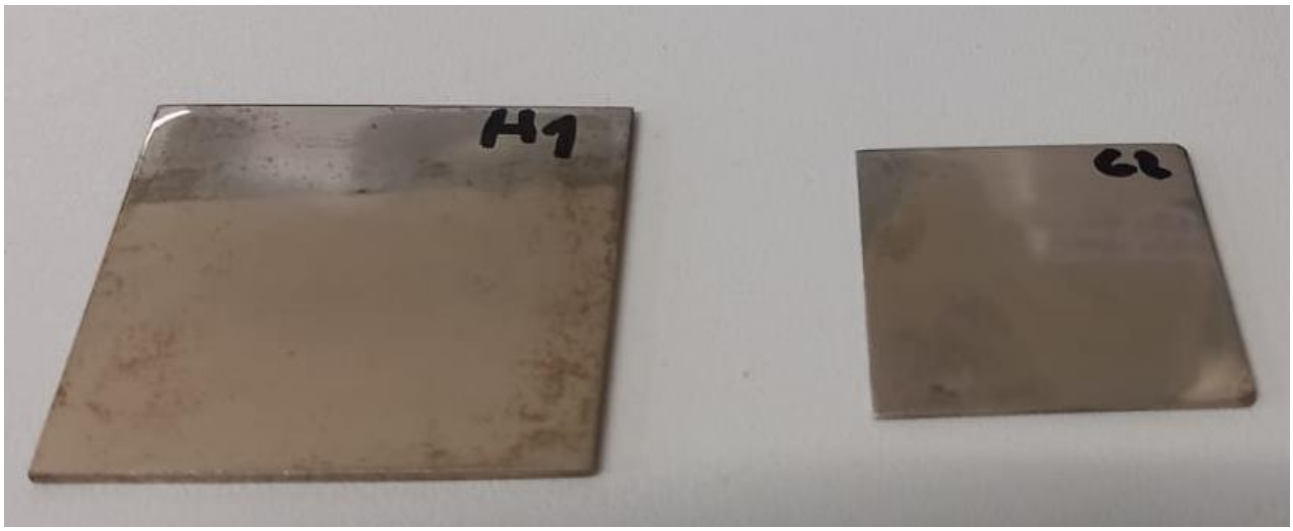

Figure 15: Visual comparison between the two coating conditions after permeation.

Another point to notice, is the integrity of the nickel layer during all the permeation. The permeated area resisted the corrosive environment for a very long time as observed from figure 15. The integrity and homogeneity of the nickel layer is vital during the permeation.

For the purpose of this study, a palladium coating could be applied. Some research works use this type of coating in their works although it is a more expensive method on coating the detection side of the sample. In this research, this method was considered but was readily abandoned due to the poor results achieved and the costs associated. The advantage of the palladium coating would be that it would allow the sample to be coated inside the permeation cell with no air exposure. On the other hand, the process would leave palladium particles inside the cell that would contaminate the whole process.

The nickel coating was achieved in a cost-effective manner at room temperature which is desirable when working with steel where temperature can influence the microstructure. Good agitation and nice electrolyte conditioning was essential to avoid bubbles in the surface of the coated layer.

4.4. Uncoated Layer

The uncoated surface of the sample, which corresponds to the charging side, the surface suffered some degree of corrosion in a specific area of the sample. This area corresponds to the top of the circumference.

During the permeation it was noticed that the electrolyte level in the chamber would go down. It was readily corrected when noticed, but still, there was some degree of exposure to the air, and it was sufficient to react with the sample resulting in the burn like corrosion shown in figure 16.

The non-permeated area evidences a darker tone, explained by the contact with the air and moisture outside the o-ring area.

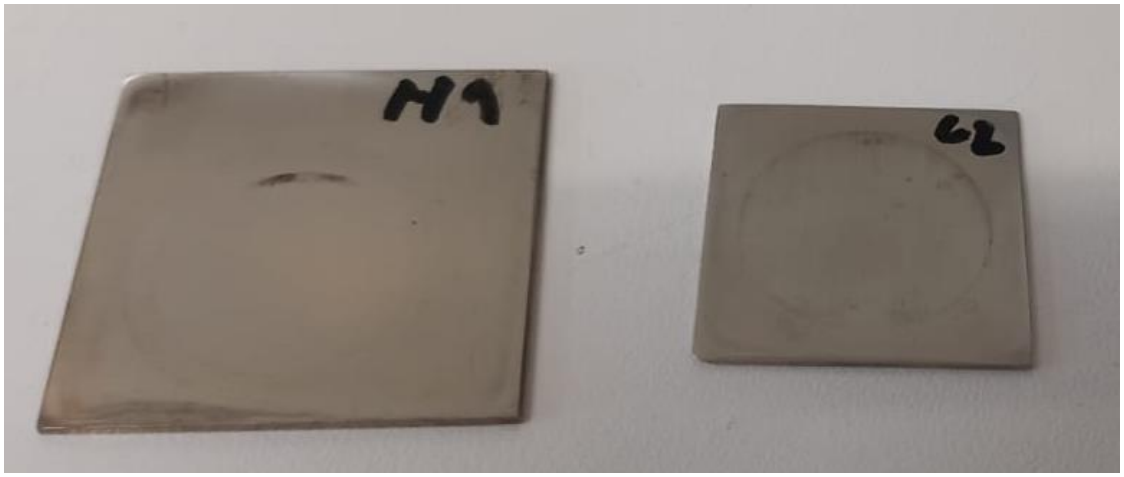

Figure 16: Visual examination of the charging side of the samples after permeation.

4.5. Permeation Results

The first permeation started by applying a 10 mA/cm2 in each sample, on the charging side and continued with a set of raises and decays in the charging current as it is detailed in appendix A. The G2 sample received a continuous permeation set of currents while the H1 sample received a twostep permeation set. The aim of the two steps in H1, intended to make sure that the reference electrode was working properly during a long permeation, in order to measure the lattice diffusion coefficient accurately. The permeation graphs are shown in graph 4, were the dashed lines correspond to changes in the permeation current.

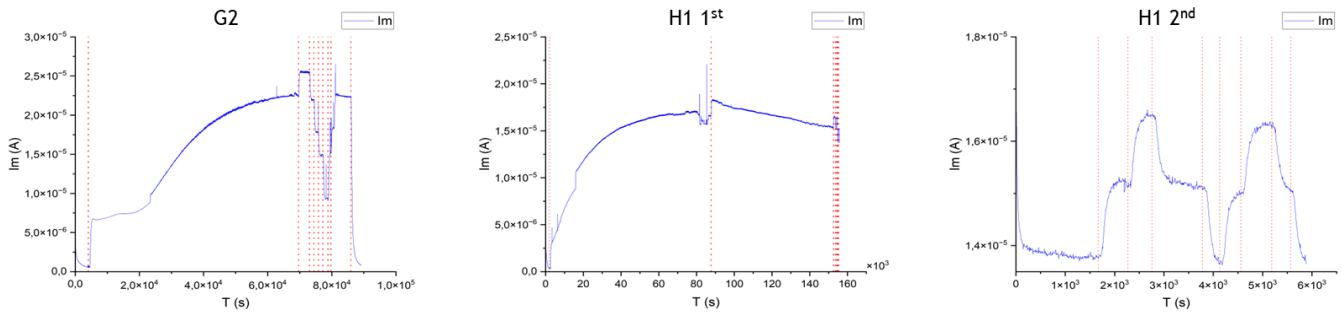

Graph 4: Permeation graphs marked with the current transitions on the charging side (dashed red lines).

Between the two sets of permeations in H1, it is expected that some hydrogen can be released from weaker traps. This does not configure an issue because, in the second permeation step, sufficient time was given to ensure that those traps are filled again. Also, the background current in the second step will not achieve the lower values seen in the first step, as expected. This happens due to the detrapping effect that is supposed to occur in the weak traps that will release a small amount of hydrogen through the membrane.

It is noticeable for both samples that after a long first permeation time, the currents obtained in each raise and decay are similar for the same permeation current. That is the expected result if the hydrogen traps are filled.

In graph 4, the dashed red lines correspond to the transitions in the permeation current imposed with the galvanostat and are detailed in appendix A.

Although the steady state currents are similar for the same permeation currents, it is noticeable that they are not equal, and that is especially true in the first couple of permeations. Also, it is noticeable that for the same transition between permeation currents (for example from a decay of 12 mA/cm^2 to 10 mA/cm^2 and a raise from 10 mA to 12mA/cm^2) the curves formed show a different behaviour.

These differences were expected because of the detrapping effect in weaker traps. Hydrogen will preferably bond to the hard traps, with higher bonding energy, and that process is irreversible, and it is expected to occur during the first permeation. On the other hand, the same does not apply to weaker traps where hydrogen can detrapp when the permeation current suddenly decreases. The opposite will happen when the current is raised again, and the trapping on the free traps will occur gain. After a long time it is expected that the trapping and detrapping in the weaker traps will reach an equilibrium and the curves and steady state currents will be more and more similar as the experiment time goes on. This effect can be observed in graph 4, as expected, when focusing on the last permeations for each sample, the steady state currents obtained, for the same permeation currents, are more similar than the first ones.

4.6. Background Current Analysis

The hydrogen permeation started after a stable background current under 2 μA/cm^2 was achieved. For H1 and G2 this happened at very small absolute background current values, 250 nA and 564 nA respectively.

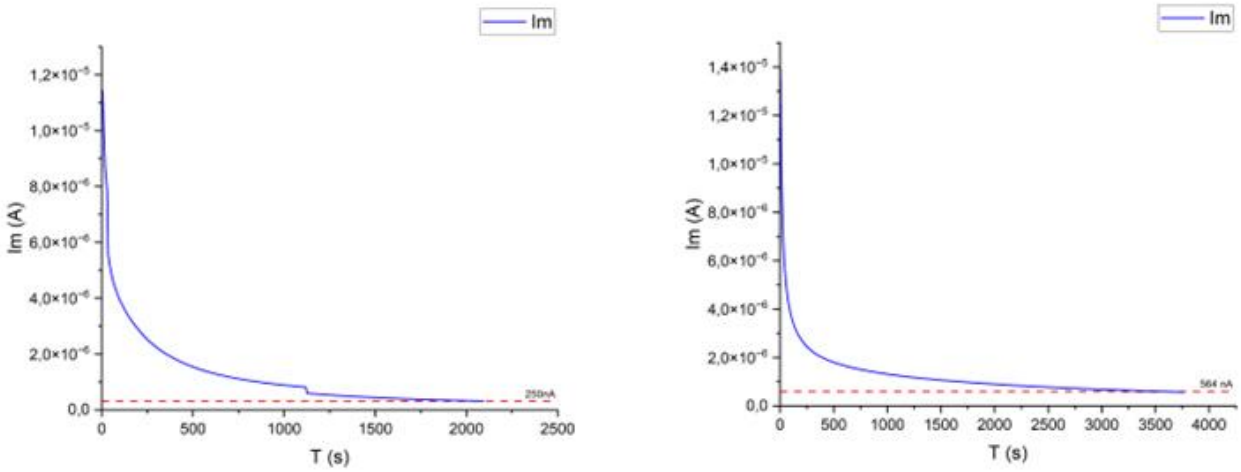

Graph 5: Pre-permeation background current for H1 and G2.

From the ASTM G-0148 and other bibliographic resources, it is known that the background currents should be under 2 μA/cm^2. The absolute background current values obtained are even smaller than the ones needed to proceed with the experiment.

The background current is achieved when the extent of the corrosion reactions at the metal surfaces is very small and gives an indication of equilibrium to ensure that the currents measured in the subsequent permeation are a consequence of the oxidation of hydrogen that reaches the detection cell. Such small and steady values can be attributed to two major factors: a very good surface condition and an effective and uniform coating.

4.7. First Permeation Results

The first permeation, as referred before, started after achieving the background current, imposing a 10 mA/cm^2 current to the system on the charging side. This current is generated in the galvanostat that ensures the stability of the current during all the permeation time.

This first permeation allowed to evaluate the effective diffusion coefficient as shown in table 6.

Table 6: Effective diffusion coefficients measured by the three different methods for G2 and H1.

Sample	i_0	i_{inf}	i_b	i_L	Breakthrough time	Lag Time	D_B	D_L	D_F
G2	0.12	5.1	2.31E-6	1.5E-5	606	27417	6.90E-7	3.89E-8	4.18E-8
H1	0.07	3.75	1.70E-06	1.07E-5	535	14024	1.22E-6	1.19E-7	1.10E-7

The coefficient was determined using three different methods. This way, the three values obtained can be compared to validate the methods. In this work, the main focus was the curve fitting method and, since there is no data to compare the results of the method with other bibliographic works, the best way to validate the results was by applying other proven methods and compare the results.

It was estimated the lag time and the breakthrough time. From that point, equations 4 and 5 were applied and the diffusion coefficient was determined. Additionally, the curve fitting method was applied using MatLab to compute the diffusion value. This iterative process works by plotting the fitting equation were the diffusion coefficient is unknown and, after applying thousands of values, the code is set to choose the coefficient values that has the best fit to que data from the permeation. In equation 6 and 7 the fitting equation is described.

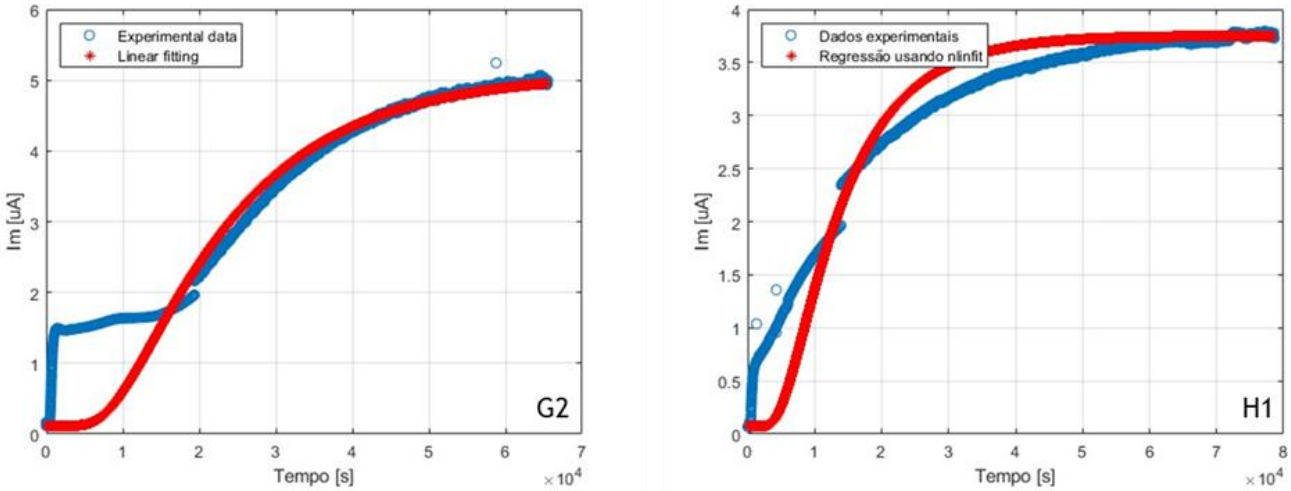

Graph 6: Curve fitting of the first permeation using MatLab for samples G2 and H1.

The obtained value by the breakthrough method was not in agreement with the values obtained from the fitting curve and the time lag method, in both experiments. The proximity between the values in two of the methods employed will serve the purpose of validation of the results. That said, in both samples two methods were validated with success and an effective diffusion coefficient value was found in each sample for the following calculations.

Methods based on time are easier to apply and give faster results but, at same time, are more subjective than the fitting method, which is based in a more precise mathematical method.

For comparison, the effective diffusion coefficient values referred in section 2.3., table 3, were used. The API 5L grade B steel is not a very common material in permeation studies. For this reason, the comparison made is based on structural similarity.

The values obtained were similar to the ones determined in previous studies for steels with a ferrite and pearlite microstructure. The G2 sample, shown a very similar effective diffusion coefficient, to the ones exposed in table 2. The same is true for the H1 sample, although the results are not as close to the effective diffusion values found for other grades of steel in the API 5L standard.

4.8. Lattice Diffusion Coefficient

After the first permeation, the lattice diffusion coefficient was determined using the linear fitting in all the subsequent permeation curves, for H1. It was shown that, as the sequence of current raises and decays succeed over time, the lattice diffusion coefficient tends to a stable value. For the lattice diffusion coefficient, only this sample was considered due to the higher permeation time employed and the thinner nickel layer.

As the permeations went by, the value of the diffusion coefficient tends to $1.11\ 10^{-5}$ cm^2/s. This value is an average between the last five permeations. In appendix B, the diffusion coefficient measured in each permeation is shown in detail.

This tendency for a certain coefficient value, for a very long time, in different permeations, indicates a state where the equilibrium in weak traps was obtained and the rate of trapping and the trapping in such locations is not significant to the lattice diffusion assessment. At this point, it is supposed that, almost all hydrogen measured in the detection side, is diffusible hydrogen that permeates trough the lattice of the steel.

The value obtained could not be compared with the values in the referred bibliography due to the lack of information in this matter. Usually, authors address the lattice diffusion coefficient as the value found for pure ferrite. This value is a pure estimate for the purpose of calculus, as many authors refer in their works.

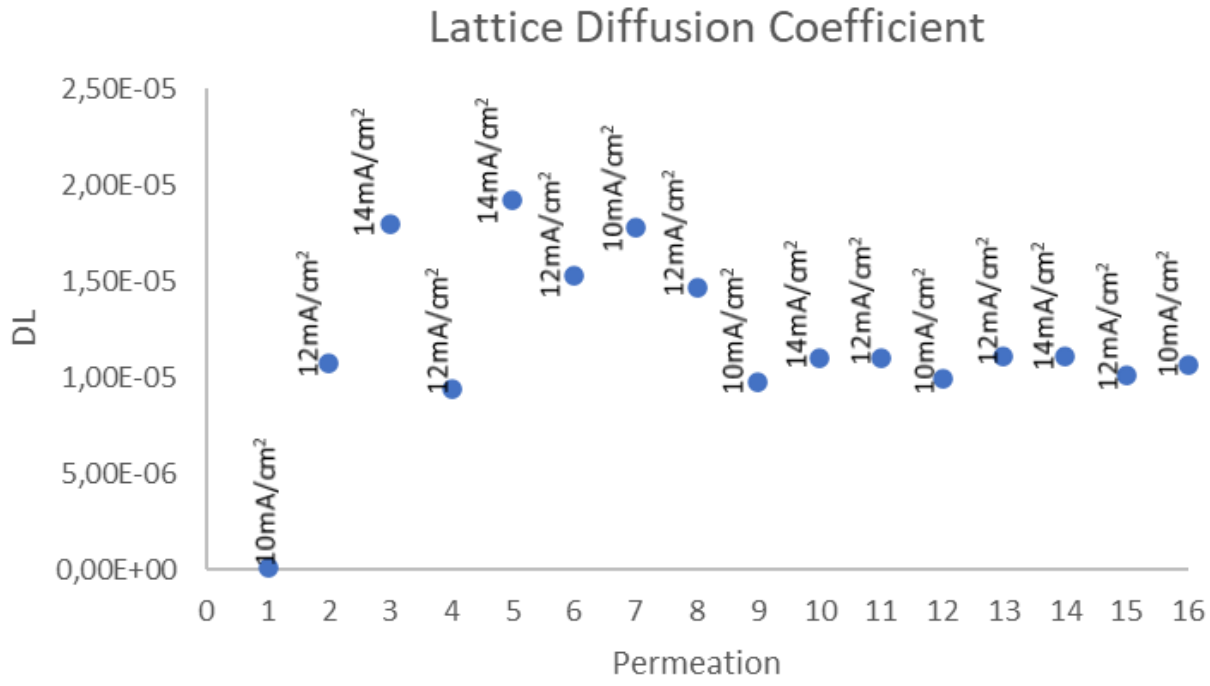

Graph 7: Plot of the different lattice diffusion coefficients measured during each permeation.

4.9. Subsurface Hydrogen Concentration, Flux and Rate

Using equation 1, 2 and 3, the hydrogen flux, rate and subsurface concentration was measured for each sample.

Table 7: Hydrogen flux, rate and subsurface concentration.

Sample	JH (molH cm^2/ s)	JHL (molH cm s)	C_0 (mol H/cm^3)
G2	2.64 10^{-11}	2.64 10^{-12}	2.32 10^{-5}
H1	1.94 10^{-11}	1.94 10^{-12}	1.70 10^{-5}

In the final stage of this work, the subsurface hydrogen concentration was obtained recurring to the equations stated before. Those values were compared with the ones found for steels in the API 5L standard with a similar ferrite and pearlite microstructure.

The subsurface concentration values found were close to the ones referred in section 2.3., table 2. A small difference can be expected due to the microstructural characteristics and composition of the material. Also, the working conditions of the base material and the sampling process will have a major impact in the final concentration.

It is known that many factors can influence the diffusion values. Between the major factors that can influence the measured hydrogen concentration in the steel after permeation are dislocations, accumulation of tensions and grain boundaries as described before. The tested samples were obtained from a working pipe and undergo a sequence of processes to retrieve the material in the form of flat and squared steel membranes. These processes will add distortions and promote the accumulation of tensions in the microstructure of the steel samples.

5. Conclusions

The conditions for the electrodeposition of nickel at room temperature were achieved. In this work it was found an optimal set of operations for this coating that allowed the expected background current to be reached.

After numerous tries, it was found that some aspects of the deposition were of major importance in the process: cleaning process, current applied and agitation.

The cleaning agents must be used in a way that ensures that the surface is completely clean prior to the electrodeposition process, detergents and alcohol are the best fit for this process and is of absolute importance that the exposure to air between steps is minimal. Another aspect to consider when cleaning the steel is the exposure to HCl, a common choice when cleaning steels, that is detrimental to the coating process and the permeation itself, therefore should not be applied.

It was found an optimal current of 3 A/dm^2 and the time of deposition can be estimated based on the area of deposition. This current must be maintained stable during all the process in order to apply the Faraday equation and achieve the thickness intended for the nickel layer.

Agitation played a big role in the process. It is responsible for preventing the appearance of pits in the nickel layer that could compromise the integrity of the continuous layer of coating that is absolutely needed for the accuracy of the results. This agitation must be mild to prevent the appearance of bubbles related with exaggerated stirring.

This coating conditions allowed a smooth layer of nickel deposited on the oxidation side that maintained the integrity during all the permeation process. In these conditions, it was possible to predict the thickness of the layers obtained, 0.05 µm for H1 and 0.41 µm for G2.

The background current must be under 2 mA/cm^2 and stable. In this experiments, the background currents achieved even smaller values and were stable before the permeations started. This can be attributed to two major factors: the cleaning process was effective, and the layer of nickel is uniform and covers the whole permeation area.

The effective diffusion coefficient was calculated by three different methods. The primary method of this work was the curve fitting which data was not available for comparison. That said, the calculations recurring to other two proven methods could validate the results of the curve fitting and, at same time, give a perception of how accurate the time lag and breakthrough methods could be in this kind of experiment.

It was found that the values obtained using the time lag method were close to the ones obtained using the curve fitting. This could help to conclude that the curve fitting obtained is accurate and no errors were committed when inputting the fitting equations in the MatLab software. Some degree of difference was expected between values due to

the subjectivity of the methods based on time. Although, the breakthrough method could not pair with the other two in terms of accuracy as it was expected from the previous works described in the literature comparing the three methods.

It was found an effective diffusion coefficient of 4.18 10^{-8} cm^2/s for the G2 sample and 1.10 10^{-7} cm^2/s for the H1 sample. These values are similar to the ones found in previous studies for the same grade of steels, with a similar microstructure.

In previous studies the lattice diffusion coefficient was estimated calculation purposes. In this study, sufficient time was given during the permeation in order to determine the lattice diffusion coefficient accurately. It was estimated a 1.11 10^{-5} cm^2/s lattice diffusion coefficient.

For the subsurface concentration of hydrogen, it was found a value of 2.32 10^{-5} mol H/cm^3 for G2 and a value of 1.70 10^{-5} mol H/cm^3 for H1. Those values are higher than the ones referred in the bibliography for steels in the API 5L standard. These differences could be explained due to the differences in the microstructure of the steels, the tensions added during the sampling process and the characteristics of the coatings applied in different works.

6. Future Works

In the course of this study several aspects of the experiments were improved and some others were found that could be perfected. The major improvements to be implemented would be in the design of the permeation cell and the sampling method.

The sampling method applied, as referred during this work, could lead to the development of tension inside the material which will influence the retention of hydrogen inside the steel. Another way to perform the sampling would be by cutting the tube in an area that is far from the permeation site and carry the test without changing the tubular shape.

This leads to another modification: the permeation cell should be designed to accommodate a tubular shape. This could not be done with the entire tube but, instead, with a section of it. Furthermore, in terms of the cell design, another aspect that should be taken into account is a feeding mechanism to maintain the level of the electrolyte to avoid the contact of the permeation are with atmospheric air that leads to a small mark of corrosion in the sample when the level of electrolyte drops.

Now that the method is established, it would be of major interest to produce the same experiment varying the sample thickness, the thickness and nature of the coating and recording pressures and temperatures.

With pressure and temperature measures, other equations found in the bibliography could be applied and the results could be compared.

Another experimental step that could be added is the live measuring of the diffusion coefficients by developing a source code that could receive the data points of the permeation and calculate the coefficients and flux in any given instant. This would give a perception of the state of the experiment without the need to proceed until the end in the case that something is not going as predicted.

References

1- Maradin, D. (2021). ADVANTAGES AND DISADVANTAGES OF RENEWABLE ENERGY SOURCES UTILIZATION. *International Journal of Energy Economics and Policy*, *11*(3), 176–183. https://doi.org/10.32479/ijeep.11027

2- Widera, B. (2019). Renewable hydrogen as an energy storage solution. E3S Web of Conferences, 116, 00097. https://doi.org/10.1051/e3sconf/201911600097

3- Van Der Spek, M., Banet, C., Bauer, C., Gabrielli, P., Goldthorpe, W., Mazzotti, M., Munkejord, S. T., Røkke, N. A., Shah, N., Sunny, N., Sutter, D., Trusler, J. M., & Gazzani, M. (2022). Perspective on the hydrogen economy as a pathway to reach net-zero CO2emissions in Europe. Energy & Environmental Science, 15(3), 1034–1077. https://doi.org/10.1039/d1ee02118d

4- The hydrogen colour spectrum. (n.d.). National Grid Group. https://www.nationalgrid.com/stories/energy-explained/hydrogen-colour-spectrum

5- Acciona. "What Are the Colours of Hydrogen and What Do They Mean?" Accessed in June 2023. https://www.acciona.com.au/updates/stories/what-are-the-colours-of-hydrogen-and-what-do-they-mean/.

6- European Commission. "Fact Sheet: Questions and Answers on the New EU Rules on Data Protection." Accessed June 2023. https://ec.europa.eu/commission/presscorner/detail/el/MEMO_18_6545.

7- European Commission. "Hydrogen." Accessed June 2023. https://energy.ec.europa.eu/topics/energy-systems-integration/hydrogen_en.

8- Zafra, A., Harris, Z. D., Sun, C., & Martínez-Pañeda, E. (2022b). Comparison of hydrogen diffusivities measured by electrochemical permeation and temperature-programmed desorption in cold-rolled pure iron. Journal of Natural Gas Science and Engineering, 98, 104365. https://doi.org/10.1016/j.jngse.2021.104365

9- Eliezer, D., & Silverstein, R. (2018). Recent studies of hydrogen embrittlement in structural materials. Procedia Structural Integrity, 13, 2233–2238. https://doi.org/10.1016/j.prostr.2018.12.135

10- Li, X., Ma, X., Zhang, J., Akiyama, E., Wang, Y., & Song, X. (2020). Review of Hydrogen embrittlement in metals: hydrogen diffusion, hydrogen characterization, hydrogen embrittlement mechanism and Prevention. Acta Metallurgica Sinica (English Letters), 33(6), 759–773. https://doi.org/10.1007/s40195-020-01039-7

11- Alcantar-Martínez, L. M., Ruiz-Trabolsi, P. A., Tadeo-Rosas, R., Miranda-Hernández, J. G., Terán-Méndez, G., Velázquez, J. C., & Hernández-Sánchez, E. (2023). Improving the surface properties of an API 5L Grade B pipeline steel by applying the boriding process. Part I: Kinetics and layer Characterization. Coatings, 13(2), 298. https://doi.org/10.3390/coatings13020298

12- Soeiro, J. C., Junior, Da Rocha, D. R., & Brandi, S. D. (2013). Uma breve revisão histórica do desenvolvimento da soldagem dos aços API para tubulações.

Soldagem E Inspeção, 18(2), 176–195. https://doi.org/10.1590/s0104-92242013000200011
13- Nasrazadani, S., Akhtar, M. A., Patel, A., & Ezell, C. (2018). Failure analysis of API 5L (Grade B) Oil Field separator Flowline pipe. Journal of Failure Analysis and Prevention, 18(4), 721–726. https://doi.org/10.1007/s11668-018-0454-0
14- Arenas-Salcedo, J. G. (2020). Effect of carbon content and microstructure on the diffusion of hydrogen in low carbon steels. International Journal of Electrochemical Science, 15(11), 11606–11622. https://doi.org/10.20964/2020.11.39
15- Liu, Q., Venezuela, J., Zhang, M., Zhou, Q., & Atrens, A. (2016). Hydrogen trapping in some advanced high strength steels. Corrosion Science, 111, 770–785. https://doi.org/10.1016/j.corsci.2016.05.046
16- Souza, R. C., Pereira, L., Starling, L. M., Pereira, J. N., Simões, T. A., Gomes, J. O., & Bueno, A. H. S. (2017). Effect of Microstructure on Hydrogen Diffusion in Weld and API X52 Pipeline Steel Base Metals under Cathodic Protection. International Journal of Corrosion, 2017, 1–14. https://doi.org/10.1155/2017/4927210
17- Xue, H., & Cheng, Y. F. (2011). Characterization of inclusions of X80 pipeline steel and its correlation with hydrogen-induced cracking. Corrosion Science, 53(4), 1201–1208. https://doi.org/10.1016/j.corsci.2010.12.011
18- Li, H., Venezuela, J., Zhou, Q., Shi, Z., Dong, F., Yan, M., Knibbe, R., Zhang, M., & Atrens, A. (2022). Effect of cold deformation on the hydrogen permeation in a dual-phase advanced high-strength steel. Electrochimica Acta, 424, 140619. https://doi.org/10.1016/j.electacta.2022.140619
19- Camero, S. (2004). Influencia del acabado superficial en la permeación de hidrógeno del acero API 5L-X52. Dialnet. https://dialnet.unirioja.es/servlet/articulo?codigo=893052
20- Standard practice for evaluation of hydrogen uptake, permeation, and transport in metals by an electrochemical technique. (n.d.). https://www.astm.org/g0148-97r18.html
21- Wang, Z., Liu, J., Huang, F., Bi, Y., & Zhang, S. (2020). Hydrogen diffusion and its effect on hydrogen embrittlement in DP steels with different martensite content. Frontiers in Materials, 7. https://doi.org/10.3389/fmats.2020.620000
22- Nickel Institute. (ca. 2023). Nickel plating handbook. nickel institute. https://nickelinstitute.org/media/lxxh1zwr/2023-nickelplatinghandbooka5_printablepdf.pdf
23- Badarulzaman, N. A., Mohamad, A. A., Puwadaria, S., & Ahmad, Z. A. (2010). The evaluation of nickel deposit obtained via Watts electrolyte at ambient temperature. Journal of Coatings Technology and Research, 7(6), 815–820. https://doi.org/10.1007/s11998-010-9271-4
24- Kim, K. B., Park, K., & Lee, J. S. (1998b). Hydrogen permeation behavior of nickel electroplated AISI 4340 steel. Metals and Materials, 4(5), 1013–1016. https://doi.org/10.1007/bf03025970

Appendix A

Sample H1	Charge/Permeation																	no charge
current density mA/cm2	10	12	14	12	14	12	10	12	10	12	14	12	10	12	14	12	10	0
time Ks	2,1	87,75	152,6	153,6	154	154,5	154,9	155,2	155,6	156/1,670	2,27	2,76	3,795	4,13	4,56	5,185	5,57	5,995
current applied A	0,045216	0,054259	0,063302	0,054259	0,063302	0,054259	0,045216	0,054259	0,045216	0,054259	0,063302	0,054259	0,045216	0,054259	0,063302	0,054259	0,045216	0
Area cm2	4,5216																	
Setup current	0,045	0,055	0,064	0,055	0,064	0,055	0,045	0,055	0,045	0,055	0,064	0,055	0,045	0,055	0,064	0,055	0,045	0
Background current	250nA/317nA																	

Sample G2	Charge/Permeation									no charge
current density mA/cm2	10	12	10	7	5	2	5	7	10	0
time Ks	4,09	69,64	73,03	74,43	75,8	77,22	78,83	79,72	80,7	85,96
current applied A	0,045216	0,054259	0,045216	0,031651	0,022608	0,009043	0,022608	0,031651	0,045216	0
Area cm2	4,5216									
Setup current	0,045	0,055	0,045	0,032	0,023	0,009	0,023	0,032	0,045	0
Background current	564nA									

Appendix B

Permeation	RISE/DECAY	Dapp (fitting) cm^2/s
1ª 0-10mA	R	1,10E-07
2ª 10mA-12mA	R	1,08E-05
3ª 12mA-14mA	R	1,80E-05
4ª 14mA-12mA	D	9,39E-06
5ª 12mA-14mA	R	1,92E-05
6ª 14mA-12mA	D	1,53E-05
7ª 12mA-10mA	D	1,78E-05
8ª 10mA-12mA	R	1,47E-05
9ª 12mA-10mA	D	9,74E-06
2ª 12mA-14mA	R	1,10E-05
3ª14mA-12mA	D	1,10E-05
4ª12mA-10mA	D	9,96E-06
5ª10mA-12mA	R	1,11E-05
6ª12mA-14mA	R	1,11E-05
7ª14mA-12mA	D	1,01E-05
8ª12mA-10mA	D	1,06E-05
9ªdescarga	D	6,30E-06